Free Radical Generation from High Frequency Electromechanical Dissociation of Pure Water

Amgad R. Rezk,[†] Heba Ahmed,[†] Tarra L. Brain,[†] Jasmine O. Castro,[†] Ming K. Tan,[‡] Julien Langley,[¶] Nicholas Cox,[¶] Joydip Mondal,[§] Wu Li,[§] Muthupandian Ashokkumar,[§] and Leslie Y. Yeo[*,†]

[†]*Micro/Nanophysics Research Laboratory, School of Engineering, RMIT University, Melbourne, VIC 3000, Australia*

[‡]*School of Engineering, Monash University Malaysia, 47500 Bandar Sunway, Selangor, Malaysia*

[¶]*Research School of Chemistry, The Australian National University, Canberra, ACT 2601, Australia*

[§]*School of Chemistry, University of Melbourne, VIC 3010, Australia*

E-mail: leslie.yeo@rmit.edu.au

Abstract

We reveal a unique mechanism by which pure water can be dissociated to form free radicals without requiring catalysts, electrolytes or electrode contact by means of high frequency nanometer-amplitude electromechanical surface vibrations in the form of surface acoustic waves (SAWs) generated on a piezoelectric substrate. The physical undulations associated with these mechanical waves, in concert with the evanescent electric field arising from the piezoelectric coupling, constitute half-wavelength 'nano-electrochemical cells' in which liquid is trapped within the SAW potential minima with vertical dimensions defined by the wave amplitude ($\approx$ 10 nm), thereby forming highly confined polarised regions with intense electric field strengths that enable the break-down of water. The ions and free radicals that are generated rapidly electromigrate under the high field intensity in addition to being convectively transported away from the cells by the bulk liquid recirculation generated by the acoustic excitation, thereby overcoming mass transport limitations that lead to ion recombination.

TOC Graphic

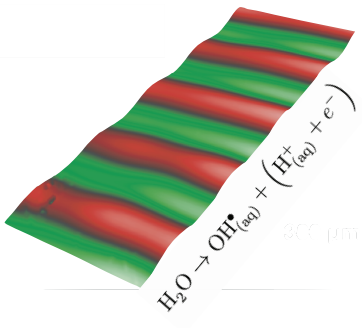

keywords: free radicals, acoustics, dissociation, piezoelectricity, sonochemistry

The search for a more efficient means for the production of free radical species such as $H^{\bullet}$, $OH^{\bullet}$ and $OOH^{\bullet}$, among others,[1] for the breakdown of perfluorinated substances, textile dyes and other pollutants[2,3] as a means for environmental remediation, and hydrogen as a renewable and sustainable energy source as an alternative to fossil fuels,[4] has motivated renewed interest in the dissociation of water. The free energy required to cleave the H–O–H bonds can be drawn from various means, including electrochemical,[5] photocatalytic[6] or sonochemical[7] reactions. Electrochemical reactions, i.e., water electrolysis,[5] remains the most widely used of these techniques. Besides requiring a suitable catalyst, high electrolyte concentrations, and, in some cases, high temperatures or pressures,[8] the necessity for the electrodes to be in contact with the bulk solution, which typically comprise highly concentrated acids/bases, make them susceptible to corrosion over time. While electrical breakdown of deionised (DI) water has been explored to directly dissociate water molecules, this typically necessitates the use of extremely large DC voltages (hundreds of kVs) to generate sufficiently high electric fields to induce the process (> 0.3 V/Å).[9]

In a recent attempt to overcome some of these issues, Wang *et al.*[10] proposed driving the electrolysis of pure (DI) water at substantially lower voltages by locally confining the electrochemical cell within a nanogap with a separation down to 37 nm that is considerably smaller than the Debye length (around 300 nm for DI water). By eliminating the existence of an electroneutral bulk Ohmic region, they were able to exploit two effects. First, the significantly larger 10^7 V/m electric field arising from the overlapping electric double layers within the nanogap (the so-called 'deep-sub-Debye-length' region) to drive ionisation of the water molecules.This is because dissociation occurs at a lower threshold electric field (i.e., a so-called 'virtual breakdown' process) significantly below that for pure water where there is a dearth of ions (i.e., 0.3 V/Å) given that there is a significantly greater ion concentration in this region by several orders of magnitude. Second, such an enhancement in the polarisation is accompanied by a concomitant increase in conductivity within this region overcomes mass transport limitations associated with ion diffusion and electromigration

across the electrodes. Their complex nanoscale electrode and nanochannel setup, nevertheless, requires elaborate fabrication. Moreover, their throughput is considerably limited owing to the confined nanoscale region where the reaction occurs. Further, the authors themselves readily admit problems associated with bubble generation that spans the nanogap across the electrodes and their tendency to corrode, which suppresses the reaction and leads to a sharp degradation in performance.

In this work, we report a surprising discovery wherein high frequency (10 MHz) nanometer-amplitude vibrations in the form of Rayleigh SAWs (electromechanical waves that are confined to and which propagate along the surface of a piezoelectric substrate) are able to drive catalyst-free dissociation of pure (DI) water at low voltages *without* the need for electrodes that are physically in contact with the water, therefore addressing many of the challenges associated with the preceding technologies. In particular, when a 10 µl DI water (resistivity 18.2 MΩ.cm; Milli-Q, Merck Millipore, Bayswater, VIC, Australia) sample, housed in a closed (sealed to minimise gas dissolution) cylindrical glass microchamber, is exposed to the acoustic excitation, i.e., the SAW, by placing it on a single crystal piezoelectric (128° Y-X $LiNbO_3$; Roditi Ltd., London, UK) substrate along which the SAW propagates (Fig. 1a,b; see Supplementary Information for details on the fabrication of the device, which was carried out in-house), we observe from the current–voltage (I–V) curves in Fig. 2 an increase in the current beyond a voltage of approximately 2.6 V, as measured through a voltage sweep using a two-wire probe station (10 µm (platinum) needle tips connected via a BNC cable to a sourcemeter (2450; Keithley Instruments, Cleveland, OH, USA)). The larger the input power applied to the SAW device, the larger the electrolytic current observed, indicating almost an order of magnitude enhancement in the electrical conductivity. We note the placement of the reservoir 5 mm away from the interdigitated transducer (IDT) electrodes (Fig. 1a,b) to which an oscillating AC signal with potentials across the range 3 to 10 V_{rms} was applied in order to generate the SAW, whose amplitude and profile is measured using a laser Doppler vibrometer (UHF-120; Polytec GmBH, Waldbronn, Germany) as seen from

the scan in Fig. 1d. The reservoir is thus sufficiently far from the IDT to prevent any electrode contact with it although within reach of the SAW transmission (Fig. 1d) given that the its attenuation length in the substrate is approximately 12 mm along its propagation direction for the 10 MHz frequency employed.[11] We also note the measurement probe wires, inserted into the reservoir as described in the Supplementary Information, were in contact with the sample only to monitor the current enhancement. The separation distance between the probes was approximately 2 mm such that any electric field generated across it is weak, thus eliminating the possibility of the participation of the probes in breakdown of the pure water sample. Heat effects are also negligible given the short exposure durations of the sample to the acoustic radiation (typically 10 s), thus limiting the temperature increase to below 5 °C even for the highest input voltage to the device, as measured using a infrared camera (Trotec EC060V; Emona Instruments Pty. Ltd., Melbourne, VIC, Australia).

The enhancement in the current above a voltage of approximately 2.6 V observed in Fig. 2, which is close to the theoretical limiting potential of 2.38 V for a one-electron water oxidation reaction:[1]

$$\mathrm{H_2O} \rightarrow \mathrm{OH^{\bullet}_{(aq)}} + \left(\mathrm{H^{+}_{(aq)}} + e^{-}\right),$$

while not ruling out the likelihood of other oxidation reactions (e.g., the two- and four-electron water oxidation reactions) taking place, suggests that the increase in the electrolytic current can be attributed to a concomitant increase in the electrical conductivity of the solution as a consequence of H^+ ion production upon irradiation of the water with the SAW. This was independently verified from measurement of the solution pH with a methyl red assay against a standard solution of 0.1 M sodium acetate/acetic acid buffer, wherein an increase in the acidity from pH 6.8 to 5.38 over a mere 10 s of SAW exposure, corresponding to a H^+ concentration of 4.2 μM, was observed (Fig. S1). Further, we note the reversibility of the process by which the SAW modulates the conductivity of the DI water in the inset of Fig. 2, wherein the conductivity can be seen to decay exponentially upon relaxation of the SAW excitation due to H^+ ion recombination. We observe though that the conductiv-

ity does not decrease to its baseline value each time, but slightly decreases on each cycle, possibly due to incremental H_2 gas production that leads to progressive trapping of bubbles at the measurement probes; such an increase in the resistance can also be seen in the onset of saturation at high voltages (10 V_{rms}) in Fig. 2. Additionally, hydrogen peroxide (H_2O_2)—generated in the other half (water reduction) reaction via consumption of the electrons produced in the one-electron water oxidation reaction above—at a concentration of approximately 15 μM, comparable to the concentration of free radicals that were produced (see below), was observed through colourimetric detection (PeroxiDetect Kit, Sigma-Aldrich Pty. Ltd., Castle-Hill, NSW, Australia).

$OH^\bullet$ free radical generation is supported by electron paramagnetic resonance (EPR) measurements. DI water samples, to which 5,5-dimethyl-1-pyrroline *N*-oxide ((DMPO) 100 μM; Sigma Aldrich Pty. Ltd., Castle Hill, NSW, Australia) radical traps were added, were exposed to the SAW and immediately pipetted into a 55 mm × 10 mm × 0.2 mm quartz flat cell and the spectra recorded (E500 X-Band Spectrometer equipped with a ER4122 SHQ Resonator; Bruker BioSpin GmbH, Rheinstetten, Germany). $OH^\bullet$ radicals were then observed following their reaction with DMPO. As can be seen in Fig. 3, the intensity of each of the four peaks associated with the DMPO–$OH^\bullet$ adduct increases with longer exposure times of the fluid to the SAW to at least 17 μM after 10 s.

Further indirect evidence of free radical generation by the SAW was obtained from methylene blue dye breakdown experiments given that $OH^\bullet$ free radicals are known to oxidise the dye, leading to its decomposition.[12] Repeated exposure of the aqueous dye solution (6.75 mg/l methylene blue (1428008; Sigma-Aldrich Pty. Ltd., Castle-Hill, NSW, Australia) in 2 ml DI water) to the SAW irradiation can be seen to progressively break down the dye, as seen from its discoloration (Fig. 4a), which was monitored using a UV-vis spectrophotometer (UV2700; Shimadzu Corp., Kyoto, Japan). The extent of dye decomposition $[(A_o - A)/A_o] \times 100\%$ was found to be approximately 94.3% after $t = 40$ mins, and follows first order kinetics $\ln[A] = \ln[A_o] - kt$ (Fig. S2 in the Supplementary Information); A_o and A are the ab-

sorbance values measured for the untreated and treated samples, respectively, and k the reaction rate constant. To verify that the decomposition occurs through a free radical pathway due to $OH^{\bullet}$ radicals generated as a consequence of the SAW-induced electrolysis of the water matrix, we repeated the decomposition experiments in the presence of dimethyl sulfoxide ((DMSO) 102952 (> 99%); Merck Millipore, Bayswater, VIC, Australia), which is a known free radical scavenger. No change in the absorption and hence decomposition of the dye was observed between the unexcited control and the sample exposed to the SAW (Fig. 4b). We thus parenthetically note the potential of the SAW platform for pollutant remediation in textile effluents and other industrial wastewater samples, especially since it does not involve the addition of photocatalysts such as TiO_2 nanoparticles that necessitate their post-treatment removal.

While bulk ultrasonic waves have been known to drive sonolytic water splitting, resulting in the formation of free radicals ($H^{\bullet}$ and $OH^{\bullet}$) and molecular products such as H_2 and H_2O_2, the physical mechanism by which this occurs is primarily via acoustic cavitation in which the large energy required to break the H–O–H bonds is supplied by that released during the violent implosion of the cavitation bubbles during which extreme temperatures ($> 10^4$ K) and pressures (> 1 GPa) are generated.[13] Indeed, acoustic cavitation has also long been invoked for a wide range of sonochemical reactions.[14,15] Nevertheless, there is a significant fundamental distinction between conventional bulk ultrasonic waves (typically driven at frequencies that are 10–100 kHz order and no greater than 3 MHz) and the SAW (typically 10 MHz and beyond) employed in the present work. Besides existing as a *surface* wave that is confined within a depth of several wavelengths (typically $\mathcal{O}$(100 μm) order) along the surface of the substrate in contrast to a *bulk* wave that is distributed and propagates throughout its thickness, cavitation is usually extremely difficult to generate at the higher ($\mathcal{O}$(10 MHz)) SAW frequency since the threshold sound intensity needed to trigger cavitation events increases rapidly with increasing frequency[16–18]—all the more given the considerably lower SAW powers employed, particularly in the water dissociation experiments in this work

($\approx$ 0.4 W), compared to that required for ultrasound ($\approx$ 20 W).[19]

We support our observations of the absence of any notable cavitation bubbles in the SAW-driven process by measuring the sonoluminescence (or lack thereof) accompanying the SAW excitation of the non-degassed DI water sample in a dark room under the same conditions, albeit in a sessile drop atop the SAW substrate open to atmosphere as opposed to within a closed microchamber, since intense light emission is well known to accompany acoustic cavitation events in pure water.[20,21] The lack of a discernible signal from a typical sonoluminescence detection setup involving a photomultiplier tube ((PMT) Hamamatsu Photonics K.K., Hamamatsu City, Shizuoka Prefecture, Japan) coupled with a high voltage power supply (Hamamatsu) and oscilloscope (Wavejet 332/334; LeCroy, Chestnut Ridge, NY)[22–24] again confirms the absence of cavitation within the limits of detection given the likelihood that the presence of dissolved gasses in the non-degassed sample acts as nucleation sites for cavitation to occur. However, as such a negative observation does not completely rule out the possibility of cavitation in its entirety, we also performed sonochemiluminescence measurements following SAW excitation of the DI water sample containing luminol solution (Sigma Aldrich Pty. Ltd., Castle Hill, NSW, Australia), whose molecules react with $OH^{\bullet}$ radicals to emit light.[25] The experiments were carried out under various atmospheric (air-saturated, air depleted and nitrogen-purged) conditions; details of the experimental method and degassing procedure can be found in the Supplementary Information. The generation of these free radicals in these experiments, albeit in the absence of cavitation, are evident from the sonochemiluminescence signals above the baseline detected using the same PMT setup (Fig. S3 in the Supplementary Information), even under air-saturated conditions where sonochemiluminescence from hydroxylated luminol may be partially quenched. Over longer exposure times beyond 1 min, we note the sonochemiluminescence signals associated with the air-depleted and nitrogen-purged conditions to approach that of the air-saturated condition (not shown) as the ambient gases eventually dissolve into the sample.

Together with the dye decomposition results in the presence of DMSO in Fig. 4b (since

cavitation is known to also result in breakdown of the dye[26]), these observations from the sonoluminescence and sonochemiluminescence experiments provide conclusive evidence to rule out the existence of cavitation and hence its role in the generation of free radicals under SAW excitation. Instead, it is possible that the evanescent electric field in the liquid region immediately adjacent to the surface of the substrate, which is associated with the electromechanical coupling of the SAW, plays a role in the dissociation of the DI water. Such fields have already been observed to be responsible for a range of SAW microfluidic actuation[27–31] phenomena, such as on-chip nanotube or nanowire manipulation, including their alignment and deagglomeration;[32–39] aerosol charging;[40] bandgap manipulation and exfoliation of piezoelectric two-dimensional nanomaterials;[41–43] and molecular orientation of crystal lattices.[44] Nevertheless, this evanescent electric field alone, which alternates every half wavelength ($\lambda_{\mathrm{SAW}} = 396$ μm at 10 MHz) and which constitutes the virtual electrodes that drive the electrolytic process (Fig. 1c), is, in itself, inadequate to directly induce the breakdown of pure water.

We thus postulate that the full electromechanical coupling is involved in the water dissociation process. As depicted in Fig. 1c, the surface undulation as the SAW traverses the substrate creates 'valleys' that constitute 'nanoelectrochemical cells' with depths commensurate with the SAW amplitude ($\sim$ 10 nm) that facilitate the physical trapping of water within highly polarised deep-sub-Debye-length confinement zones. These zones are akin to the nanogap electrochemical cells in Wang *et al.*[10], albeit dynamically created by the SAW, therefore circumventing the need for complex nanofabrication of both the nanoscale electrodes or the nanochannels that separate them. We note that the enhanced evanescent electric field in this region, typically on the order 10^8 V/m (1 V across 10 nm; see, for example, Fig. 1e, in addition to Refs. 43 and 45 where similar values for the intensity of the SAW evanescent electric field are reported), is at least comparable to, if not one order of magnitude larger than the $\mathcal{O}(10^7)$ V/m electric field across the nanogap electrode in Wang *et al.*[10] sufficient to drive self-ionisation of water as a virtual breakdown process.[9]

Moreover, the enhanced local field within the confinement of these nanoelectrochemical cells also drives fast electromigration of the ions and free radicals generated within them during each half AC cycle out into the bulk of the fluid so as to prevent their recombination during the next half cycle when the polarisation is reversed, as indicated by the short electromigration time scale $\mathcal{L}_{\mathrm{N}}RT/\mathcal{D}FE \sim 10^{-9}$ s compared to the ms to μs typical ion recombination timescale[46,47] and the μs to ns typical lifetime of the free radicals;[48] here, $\mathcal{L}_{\mathrm{N}} \sim 10^{-9}$ m is the characteristic length scale associated with the depth of the cell out of which the ions have to migrate to reach the bulk, R the molar gas constant, T the absolute temperature, $\mathcal{D}$ the ion diffusivity, F the Faraday constant and $E \sim 10^{8}$ V/m the local electric field. This is in contrast to the much longer diffusion time scale $\mathcal{L}_{\mathrm{B}}^{2}/\mathcal{D} \sim 10^{-3}$ s for conventional electrolysis in macroscopic systems in which the electric field is typically screened by the Debye layer, which means that the ions and free radicals that are generated essentially recombine before they are able to diffuse away across the bulk of the fluid to the counterelectrode over a length scale $\mathcal{L}_{\mathrm{B}} \sim 10^{-3}$ m. In addition, the acoustic streaming (non-zero time-averaged momentum flux arising from the pressure and viscous fluctuations associated with the sound wave propagation in the fluid)[49] that arises as a consequence of viscous attenuation of the energy leaked into the water phase by the SAW also plays a role in overcoming the transport limitation of the ions and free radicals generated within the cell. More specifically, the long-range convection facilitated by this acoustically-driven recirculatory flow within the fluid transports the ions and free radicals away into the bulk of the fluid while continuously replenishing the nanoelectrochemical cell regions with fresh water molecules where they further dissociate. This is confirmed by suppressing the electric field component of the SAW through the deposition of a thin gold layer on the SAW substrate (thus leaving behind only a pure mechanical wave—i.e., the acoustic component of the SAW), in which case, no free radicals (such as that evidenced in Fig. 3) were observed—a result that also provides a further distinction between the present platform and that of cavitation-induced sonolysis where free radicals are generated purely due to the mechanical

component associated with the bulk ultrasonic excitation.

In summary, we have discovered a unique mechanism by which pure water can be dissociated via the electromechanical coupling arising from MHz-order surface vibrations in the form of SAWs at low voltages without requiring catalysts or contact with electrodes. The evanescent electric field of the SAW in the water phase together with the physical waveform of the SAW on the surface of the piezoelectric substrate act in concert to produce virtual electrodes that give rise to confined regions with alternating polarities over every half wavelength. The nanometer-order vertical dimension of these virtual electrochemical cells, as stipulated by the amplitude of the SAW, is substantially below the Debye length, and therefore constitute highly polarised regions with high field intensities ($\mathcal{O}(10^8)$ V/m) that drive field-assisted self-ionisation and hence virtual breakdown of water. The ions and free radicals that are generated are then transported away from these regions by the long-range convection facilitated by the acoustic streaming that accompanies the SAW excitation of the fluid to prevent their recombination. Given the low costs (typically US$1/device by exploiting the economies of scale associated with mass nanofabrication) and chipscale dimensions of the devices, we anticipate the possibility for scaling the process to achieve industrial-scale throughput through massive parallelisation. Moreover, the free radical generation mechanism reported here could also open up entire new possibilities for cavitation-free sonochemical synthesis that was recently speculated[50] but which has yet to be demonstrated.

Acknowledgement

A.R.R., N.C and L.Y.Y. acknowledge funding support from the Australian Research Council through Discovery Project (DP180102110), Future Fellowship (FT140100834) and Linkage, Infrastructure, Equipment & Facilities (LE170100023) grants. The authors also acknowledge the use of the nanofabrication facilities and technical support at the RMIT MicroNano Research Facility (MNRF).

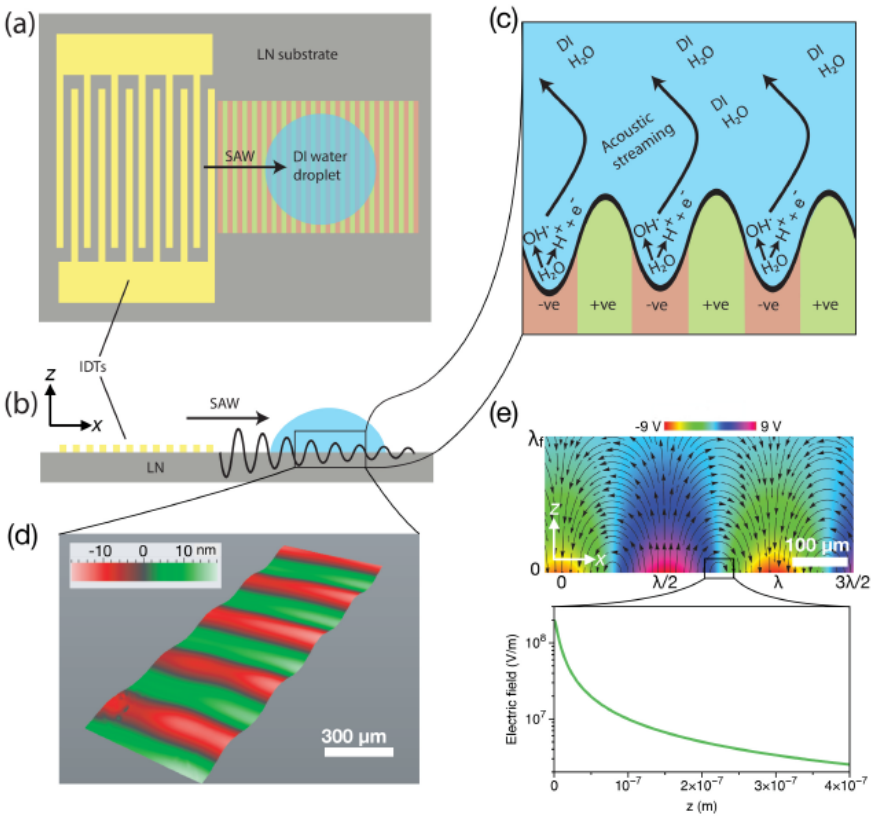

Figure 1: (a) Top and (b) side view schematics (not to scale) illustrating the experimental setup in which a SAW, generated along the piezoelectric $LiNbO_3$ substrate (LN) by applying an oscillating electrical signal to the IDT, is coupled into a 10 µl fluid reservoir (microchamber) of pure (DI) water. We note that the IDT is *not* in contact with the fluid or chamber at all times. (c) Magnified schematic (not to scale) showing the confined regions defined by the SAW substrate displacement—approximately 10 nm, as shown in the laser Doppler vibrometer (LDV) scan in (d)—which constitute nanoscale 'electrochemical cells' with high field intensities ($\mathcal{O}(10^8)$ V/m) where the water dissociation reaction occurs. These high field intensities are supported by (e) the numerical simulation (see Supplementary Information for details) of the electric potential (top) and calculation of a representative electric field profile immediately adjacent to the SAW substrate surface at $z = 0$ (bottom). λ and λ_f denote the wavelength of the SAW and the sound wave in water, respectively; we note that the dimensions of call-out box from the contour plot above is not to scale. The ions and free radicals that are generated are rapidly swept into the bulk of the fluid by electromigration effects as well as the accompanying acoustic streaming flow . Concomittantly, fresh water molecules are also continuously convected into the nanoelectrochemical cell region where they dissociate to produce more free radicals.

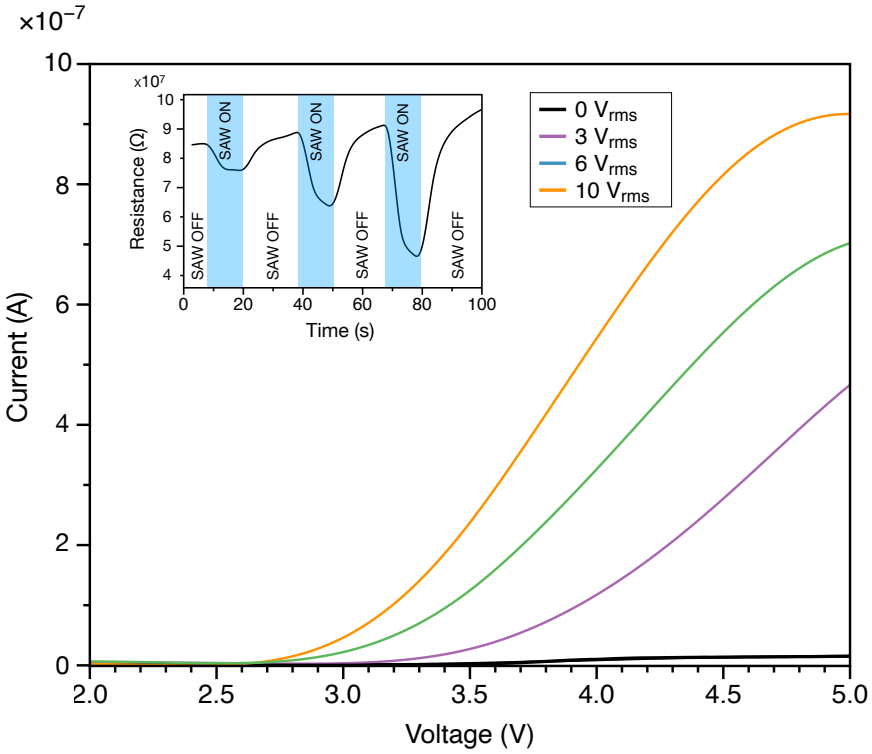

Figure 2: I–V curves for a pure (DI) water measured using a two-wire probe station. The current flow was monitored through a voltage sweep from 0 to 5 V, in the absence of the SAW and during SAW excitation for three different input voltages. The inset shows the in-situ and revrersible behavior associated with the change in electrical resistance in the fluid when the SAW is triggered on and off at the same input voltage as that used to generate the results in the main figure.

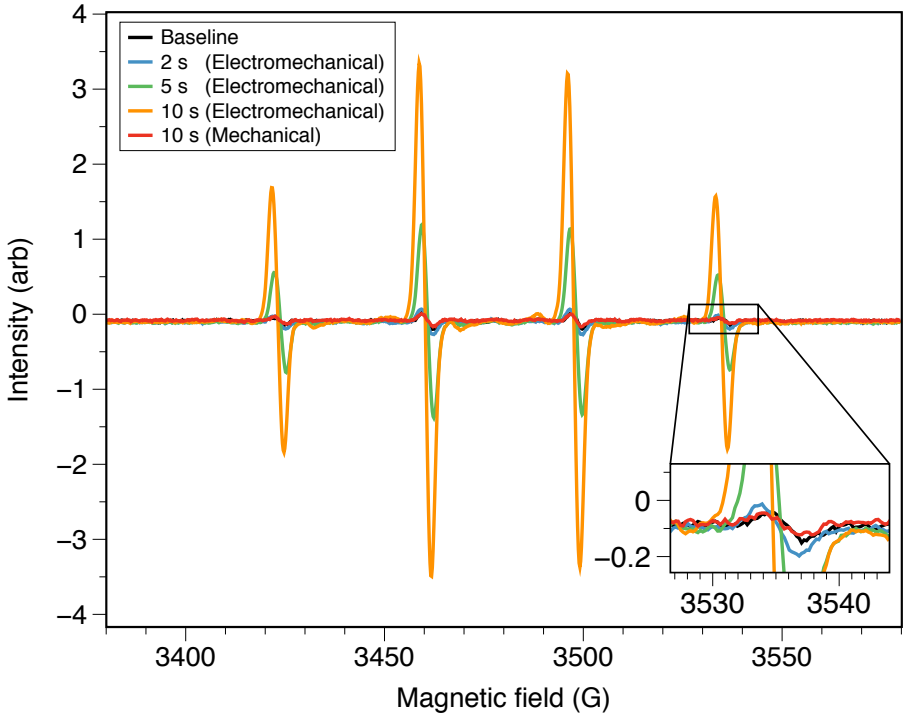

Figure 3: Electron paramagnetic resonance (EPR) measurements monitoring the concentration of the $OH^{\bullet}$ radicals formed following exposure of water to the SAW (electromechanical wave) over a duration of 2, 5 and 10 s, compared to water that was only exposed purely to its mechanical component (the electrical field associated with the SAW is shielded with a thin gold layer deposited on the SAW substrate) for 10 s in which no free radicals were produced, as compared to the baseline reading. The EPR signal observed is that of the DMPO–$OH^{\bullet}$ adduct, which allows the short lived $OH^{\bullet}$ radical to be quantified. The EPR settings are as follows: microwave frequency 9.8 GHz, power 4.74 mW, magnetic field modulation frequency 100 kHz and magnetic field modulation amplitude 0.5 G.

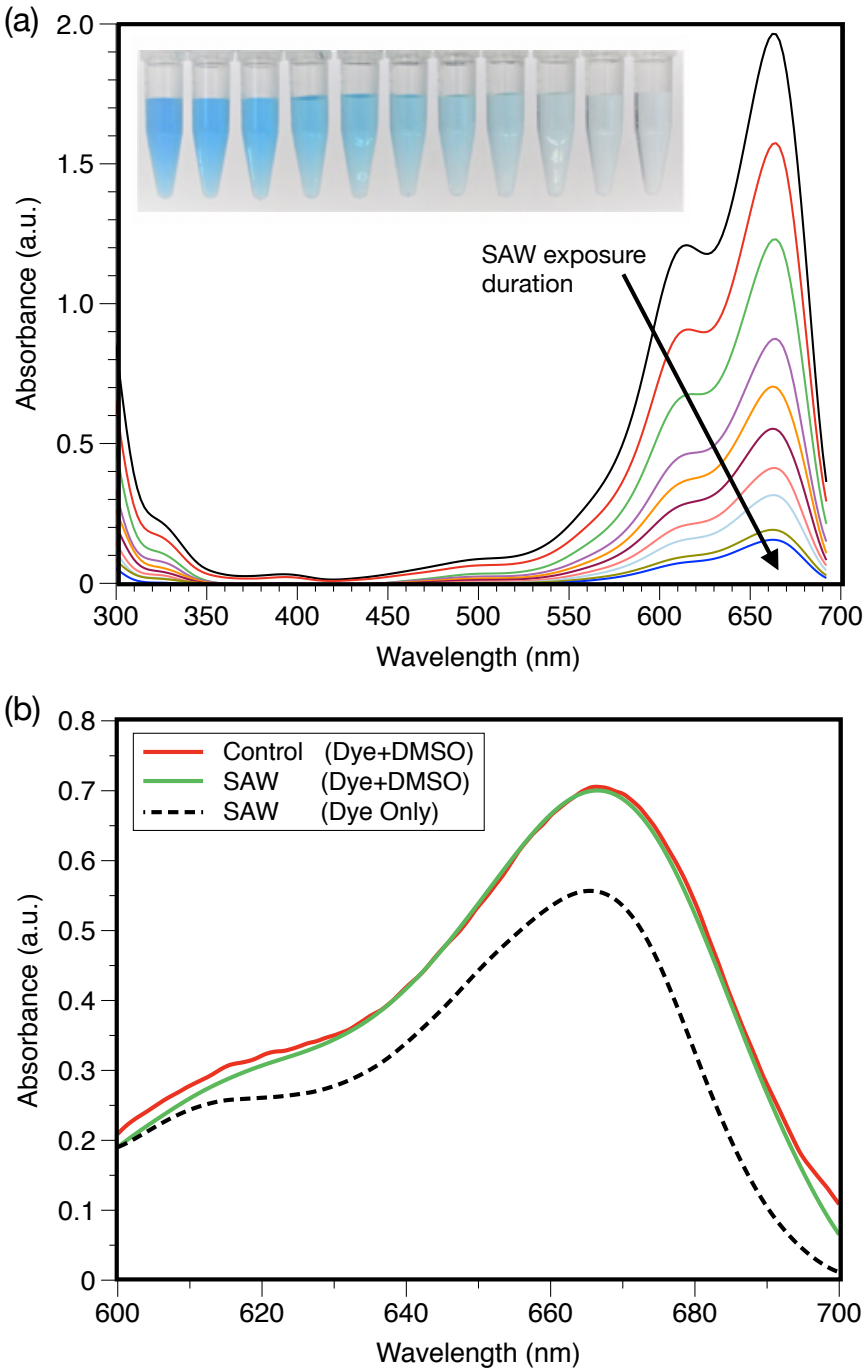

Figure 4: (a) UV–vis spectra for methylene blue dye absorption showing progressive signal reduction and hence breakdown of the dye upon continued exposure to the SAW (94.3% after 40 mins), as depicted by the images in the inset which show visual discolouration of the dye as it is progressively decomposed by the SAW. (b) Absorbance measurements showing the effect of adding a free radical scavenger (DMSO) on the dye breakdown process in which the influence of the SAW in generating the free radicals which leads to breakdown of the dye is suppressed.

References

1. Shi, X.; Siahrostami, S.; Li, G.-L.; Zhang, Y.; Chakthranont, P.; Studt, F.; Jaramillo, T. F.; Zheng, X.; Nørskov, J. K. Understanding Activity Trends in Electrochemical Water Oxidation to Form Hydrogen Peroxide. *Nat. Commun.* **2017**, *8*, 701.

2. Singh, R. K.; Fernando, S.; Baygi, S. F.; Multari, N.; Thagard, S. M.; Holsen, T. M. Breakdown Products from Perfluorinated Alkyl Substances (PFAS) Degradation in a Plasma-Based Water Treatment Process. *Environ. Sci. Technol.* **2019**, *53*, 2731–2738.

3. Vinodgopal, K.; Peller, J. Hydroxyl Radical-Mediated Advanced Oxidation Processes for Textile Dyes: A Comparison of the Radiolytic and Sonolytic Degradation of the Monoazo Dye Acid Orange 7. *Res. Chem. Intermediat.* **2003**, *29*, 307–316.

4. Chornet, E.; Czernik, S. Harnessing Hydrogen. *Nature* **2002**, *418*, 928–929.

5. Mallouk, T. E. Water Electrolysis: Divide and Conquer. *Nat. Chem.* **2013**, *5*, 362.

6. Maeda, K.; Teramura, K.; Lu, D.; Saito, N.; Inoue, Y.; Domen, K. Noble–Metal/Cr_2O_3 Core/Shell Nanoparticles as a Cocatalyst for Photocatalytic Overall Water Splitting. *Angew. Chem. Int. Ed.* **2006**, *45*, 7806–7809.

7. Morosini, V.; Chave, T.; Virot, M.; Moisy, P.; Nikitenko, S. I. Sonochemical Water Splitting in the Presence of Powdered Metal Oxides. *Ultrason. Sonochem.* **2016**, *29*, 512–516.

8. LeRoy, R. Industrial Water Electrolysis: Present and Future. *Int. J. Hydrogen Energ.* **1983**, *8*, 401–417.

9. Malik, M. A.; Ghaffar, A.; Malik, S. A. Water Purification by Electrical Discharges. *Plasma Sources Sci. Technol.* **2001**, *10*, 82.

10. Wang, Y.; Narayanan, S.; Wu, W. Field-Assisted Splitting of Pure Water Based on Deep-Sub-Debye-Length Nanogap Electrochemical Cells. *ACS Nano* **2017**, *11*, 8421–8428.

11. Ryzy, M.; Grabec, T.; Österreicher, J.; Hettich, M.; Veres, I. Measurement of Coherent Surface Acoustic Wave Attenuation in Polycrystalline Aluminum. *AIP Adv.* **2018**, *8*, 125019.

12. Wang, Z.; Zhao, H.; Qi, H.; Liu, X.; Liu, Y. Free Radical Behaviours During Methylene Blue Degradation in the Fe^{2+}/H_2O_2 System. *Environ. Technol.* **2019**, *40*, 1138–1145.

13. Merouani, S.; Hamdaoui, O.; Rezgui, Y.; Guemini, M. Mechanism of the Sonochemical Production of Hydrogen. *Int. J. Hydrogen Energ.* **2015**, *40*, 4056–4064.

14. Suslick, K. S. Sonochemistry. *Science* **1990**, *247*, 1439–1445.

15. Suslick, K. S.; Flannigan, D. J. Inside a Collapsing Bubble: Sonoluminescence and the Conditions During Cavitation. *Annu. Rev. Phys. Chem.* **2008**, *59*, 659–683.

16. Sponer, J. Dependence of the Cavitation Threshold on the Ultrasonic Frequency. *Czech. J. Phys.* **1990**, *40*, 1123–1132.

17. Okitsu, K.; Ashokkumar, M.; Grieser, F. Sonochemical Synthesis of Gold Nanoparticles: Effects of Ultrasound Frequency. *J. Phys. Chem. B* **2005**, *109*, 20673–20675.

18. Nguyen, T.; Asakura, Y.; Koda, S.; Yasuda, K. Dependence of Cavitation, Chemical Effect, and Mechanical Effect Thresholds on Ultrasonic Frequency. *Ultrason. Sonochem.* **2017**, *39*, 301–306.

19. Weissler, A. Formation of Hydrogen Peroxide by Ultrasonic Waves: Free Radicals. *J. Am. Chem. Soc.* **1959**, *81*, 1077–1081.

20. Gaitan, D. F.; Crum, L. A.; Church, C. C.; Roy, R. A. Sonoluminescence and Bubble Dynamics for a Single, Stable, Cavitation Bubble. *J. Acoust. Soc. Am.* **1992**, *91*, 3166–3183.

21. Brenner, M. P.; Hilgenfeldt, S.; Lohse, D. Single-Bubble Sonoluminescence. *Rev. Mod. Phys.* **2002**, *74*, 425–484.

22. Ashokkumar, M.; Guan, J.; Tronson, R.; Matula, T. J.; Nuske, J. W.; Grieser, F. Effect of Surfactants, Polymers, and Alcohol on Single Bubble Dynamics and Sonoluminescence. *Phys. Rev. E* **2002**, *65*, 046310.

23. Brotchie, A.; Grieser, F.; Ashokkumar, M. Effect of Power and Frequency on Bubble-Size Distributions in Acoustic Cavitation. *Phys. Rev. Lett.* **2009**, *102*, 084302.

24. Ashokkumar, M.; Lee, J.; Iida, Y.; Yasui, K.; Kozuka, T.; Tuziuti, T.; Towata, A. Spatial Distribution of Acoustic Cavitation Bubbles at Different Ultrasound Frequencies. *ChemPhysChem* **2010**, *11*, 1680–1684.

25. Hatanaka, S.-i.; Mitome, H.; Yasui, K.; Hayashi, S. Single-Bubble Sonochemiluminescence in Aqueous Luminol Solutions. *J. Am. Chem. Soc.* **2002**, *124*, 10250–10251.

26. Kumar, M. S.; Sonawane, S.; Pandit, A. B. Degradation of Methylene Blue Dye in Aqueous Solution Using Hydrodynamic Cavitation Based Hybrid Advanced Oxidation Processes. *Chem. Eng. Process.* **2017**, *122*, 288–295.

27. Friend, J.; Yeo, L. Y. Microscale Acoustofluidics: Microfluidics Driven via Acoustics and Ultrasonics. *Rev. Mod. Phys.* **2011**, *83*, 647–704.

28. Ding, X.; Li, P.; Lin, S.-C. S.; Stratton, Z. S.; Nama, N.; Guo, F.; Slotcavage, D.; Mao, X.; Shi, J.; Costanzo, F.; Huang, T. J. Surface Acoustic Wave Microfluidics. *Lab Chip* **2013**, *13*, 3626–3649.

29. Yeo, L. Y.; Friend, J. R. Surface Acoustic Wave Microfluidics. *Annu. Rev. Fluid Mech.* **2014**, *46*, 379–406.

30. Destgeer, G.; Sung, H. J. Recent Advances in Microfluidic Actuation and Micro-Object Manipulation via Surface Acoustic Waves. *Lab Chip* **2015**, *15*, 2722–2738.

31. Go, D. B.; Atashbar, M. Z.; Ramshani, Z.; Chang, H.-C. Surface Acoustic Wave Devices

for Chemical Sensing and Microfluidics: A Review and Perspective. *Anal. Meth.* **2017**, *9*, 4112–4134.

32. Strobl, C. J.; Schäflein, C.; Beierlein, U.; Ebbecke, J.; Wixforth, A. Carbon Nanotube Alignment by Surface Acoustic Waves. *Appl. Phys. Lett.* **2004**, *85*, 1427–1429.

33. Smorodin, T.; Beierlein, U.; Ebbecke, J.; Wixforth, A. Surface-Acoustic-Wave-Enhanced Alignment of Thiolated Carbon Nanotubes on Gold Electrodes. *Small* **2005**, *1*, 1188–1190.

34. Seemann, K. M.; Ebbecke, J.; Wixforth, A. Alignment of Carbon Nanotubes on Pre-Structured Silicon by Surface Acoustic Waves. *Nanotechnology* **2006**, *17*, 4529–4532.

35. Zeng, Q.; Li, L.; Ma, H. L.; Xu, J.; Fan, Y.; Wang, H. A Non-Contact Strategy for Controlled Enrichment, Manipulation, and Separation of Carbon Nanotubes by Surface Acoustic Waves. *Appl. Phys. Lett.* **2013**, *102*, 213106.

36. Kong, X. H.; Deneke, C.; Schmidt, H.; Thurmer, D. J.; Bauer, M.; Schmidt, O. G. Surface Acoustic Wave Mediated Dielectrophoretic Alignment of Rolled-Up Microtubes in Microfluidic Systems. *Appl. Phys. Lett.* **2010**, *96*, 134105.

37. Chen, Y.; Ding, X.; Steven Lin, S.-C.; Yang, S.; Huang, P.-H.; Nama, N.; Zhao, Y.; Nawaz, A. A.; Guo, F.; Wang, W.; Gu, Y.; Mallouk, T. E.; Huang, T. J. Tunable Nanowire Patterning Using Standing Surface Acoustic Waves. *ACS Nano* **2013**, *7*, 3306–3314.

38. Miansari, M.; Qi, A.; Yeo, L. Y.; Friend, J. R. Vibration-Induced Deagglomeration and Shear-Induced Alignment of Carbon Nanotubes in Air. *Adv. Funct. Mater.* **2015**, *25*, 1014–1023.

39. Ma, Z.; Guo, J.; Liu, Y. J.; Ai, Y. The Patterning Mechanism of Carbon Nanotubes

Using Surface Acoustic Waves: The Acoustic Radiation Effect or the Dielectrophoretic Effect. *Nanoscale* **2015**, *7*, 14047–14054.

40. Ho, J.; Tan, M.; Go, D.; Yeo, L.; Friend, J.; Chang, H. Paper-Based Microfluidic Surface Acoustic Wave Sample Delivery and Ionization Source for Rapid and Sensitive Ambient Mass Spectrometry. *Anal. Chem.* **2011**, *83*, 3260–3266.

41. Rezk, A. R.; Walia, S.; Ramanathan, R.; Nili, H.; Ou, J. Z.; Bansal, V.; Friend, J. R.; Bhaskaran, M.; Yeo, L. Y.; Sriram, S. Acoustic–Excitonic Coupling for Dynamic Photoluminescence Manipulation of Quasi-2D MoS_2 Nanoflakes. *Adv. Opt. Mater.* **2015**, *3*, 888–894.

42. Rezk, A. R.; Carey, B.; Chrimes, A. F.; Lau, D. W. M.; Gibson, B. C.; Zheng, C.; Fuhrer, M. S.; Yeo, L. Y.; Kalantar-zadeh, K. Acoustically-Driven Trion and Exciton Modulation in Piezoelectric Two-Dimensional MoS_2. *Nano Lett.* **2016**, *16*, 849–855.

43. Ahmed, H.; Rezk, A. R.; Carey, B. J.; Wang, Y.; Mohiuddin, M.; Berean, K. J.; Russo, S. P.; Kalantar-zadeh, K.; Yeo, L. Y. Ultrafast Acoustofluidic Exfoliation of Stratified Crystals. *Adv. Mater.* **2018**, *30*, 1704756.

44. Ahmed, H.; Rezk, A. R.; Richardson, J. J.; Macreadie, L. K.; Babarao, R.; Mayes, E. L. H.; Lee, L.; Yeo, L. Y. Acoustomicrofluidic Assembly of Oriented and Simultaneously Activated Metal–Organic Frameworks. *Nat. Commun.* **2019**, *10*, 2282.

45. Weiß, M.; Krenner, H. J. Interfacing Quantum Emitters with Propagating Surface Acoustic Waves. *J. Phys. D: Appl. Phys.* **2018**, *51*, 373001.

46. Swierk, J. R.; McCool, N. S.; Mallouk, T. E. Dynamics of Electron Recombination and Transport in Water-Splitting Dye-Sensitized Photoanodes. *J. Phys. Chem. C* **2015**, *119*, 13858–13867.

47. Takanabe, K. Photocatalytic Water Splitting: Quantitative Approaches Toward Photocatalyst by Design. *ACS Catal.* **2017**, *7*, 8006–8022.

48. Pryor, W. A. Oxy-Radicals and Related Species: Their Formation, Lifetimes, and Reactions. *Annu. Rev. Physiol.* **1986**, *48*, 657–667.

49. Lighthill, J. Acoustic Streaming. *J. Sound Vibrat.* **1978**, *61*, 391–418.

50. Vinatoru, M.; Mason, T. J. Can Sonochemistry Take Place in the Absence of Cavitation? – A Complementary View of How Ultrasound Can Interact with Materials. *Ultrason. Sonochem.* **2019**, *52*, 2–5.